ELSEVIER

PII:S0267-7261(96)00002-4

Soil Dynamics and Earthquake Engineering 15 *(1996) 337-346*

0267-7261/96/$15.00

Viscoelastic approximation of poroelastic media for wave scattering problems

V. Morochnik & J. P. Bardet

Civil Engineering Department, University of Southern California, Los Angeles, CA 90089, USA

Communicated by M. D. Trifunac

(Received 4 April 1995; revised version received 22 November 1995; accepted 12 December 1995)

Herein, we propose a simplified and approximate method for solving dynamic problems in poroelastic media. The method is based on the definition of equivalent-viscoelastic materials that have the same wave numbers as poroelastic media. The viscoelastic approximation was applied to study the scatter of plane compressional waves by a spherical poroelastic inhomogeneity. In this wave scattering problem, the poroelastic and equivalent-viscoelastic solutions gave almost identical results far away from the inhomogeneity. The proposed method extends our existing numerical and analytical methods for poroelastic media. It is useful to derive approximate analytical solutions which can be applied for assessing the damping characteristics of small amplitude waves in saturated soils. Copyright © 1996 Elsevier Science Limited.

INTRODUCTION

The scatter of body waves by inhomogeneities is a fundamental problem in soil dynamics and geophysics. After waves impinge on inhomogeneities, they reflect and refract in intricate patterns dependent on the shape and properties of the inclusion and surrounding matrix. The scatter of waves by a spherical elastic inhomogeneity in an elastic matrix was investigated by many authors, e.g., Sivukhin' and Ying & Truell.[2] The elastic solutions were extended to viscoelastic media by Gaunaurd & Überall[3] and Morochnik,[4] and to poroelastic media by Berryman.[5]

Unlike elastic media which are non-dissipative and deprived from material damping, poroelastic media such as saturated soils and rocks dissipate energy and attenuate waves. Poroelastic media possess a shear wave and two compressional waves — a slow wave which is strongly attenuated, and a fast wave which is slightly damped." Several investigators have explored the scattering of poroelastic waves. Berryman[5] analytically studied the scattered wave patterns for long wavelengths. Zimmerman & Stern[7] examined the scattering of plane compression waves by a sphere which is either rigid or composed of elastic solid or fluid, but confined their numerical examples to the close proximity of the inclusion. Kargl & Lim[8] formulated a transition matrix approach to study the waves scattered by a poroelastic inclusion, and presented some numerical examples for porous obstacles in water and superfluiddsuperleak systems. Wave scatter problems in poroelastic media[9] are complicated compared to those in viscoelastic media (e.g., Morochnik[4]), which may account for the scarcity of analytical solutions.

This paper summons the viscoelastic nature of dynamic poroelasticity" and proposes a simplified and approximate method for analyzing dynamic problems in poroelasticity. In particular, it examines the relevance of viscoelastic approximations to the problem of plane compressional waves scattered by a spherical poroelastic inclusion. Following the introduction, the second and third sections summarize the basic equations of dynamic poroelasticity, and the poroelastic solution of wave scattering problems. The fourth section reviews the basic equations of dynamic viscoelasticity, and formulates the poroelastic-viscoelastic similarity. The fifth section investigates the viscoelastic approximation by comparing poroelastic and viscoelastic numerical results. Possible applications of the present method to engineering problems are only briefly discussed before concluding.

EQUATIONS OF DYNAMIC POROELASTICITY

In the absence of body forces, the equations of dynamic

poroelasticity are:"

$$\begin{cases} N\nabla^2\mathbf{u} + \mathbf{grad}\,[(P-N)\ \mathrm{div\ u} + Q\ \mathrm{div\ v}] \\ \qquad = \tilde{\rho}_{11}\ddot{\mathbf{u}} + \tilde{\rho}_{12}\ddot{\mathbf{v}} + b(\dot{\mathbf{u}} - \dot{\mathbf{v}}) \\ \mathrm{grad(Qdivu + Rdivv)} = \tilde{\rho}_{12}\ddot{\mathbf{u}} + \tilde{\rho}_{22}\ddot{\mathbf{v}} - b(\dot{\mathbf{u}} - \dot{\mathbf{v}}), \end{cases} \tag{1}$$

where $\mathbf{u}$ is the solid displacement; v is the fluid pseudo-displacement; P, Q, R and N are Biot's elastic constants; and $\tilde{\rho}_{11}, \tilde{\rho}_{12}$ and $\tilde{\rho}_{22}$ are the mass coefficients related to the fluid and solid densities. Parameter b is a dissipative coefficient related to hydraulic conductivity k, unit mass of the fluid ρ_f, earth acceleration g, and porosity f through:

$$b = f^2 \frac{g\rho_f}{k}. \tag{2}$$

In the case of stationary problems, the solid and fluid displacements are harmonic function of the circular frequency w

$$\begin{aligned} \mathbf{u}(\mathbf{x}, t) &= \mathbf{U}(\mathbf{x})e^{-i\omega t} \\ \mathbf{v}(\mathbf{x}, t) &= \mathbf{V}(\mathbf{x})e^{-i\omega t}. \end{aligned} \tag{3}$$

After omitting the time dependency, eqn (1) becomes

$$\begin{cases} N\nabla^2\mathbf{U} + \mathbf{grad}\,[(\mathbf{P}-N)\ \mathrm{div\ U} + \mathrm{Q\ div\ V}] \\ \qquad +\omega^2(\rho_{11}\mathbf{U} + \rho_{12}\mathbf{V}) = \mathbf{0} \qquad (4a) \\ \mathrm{grad}\ (Q\,\mathrm{div}\,\mathbf{U} + R\,\mathrm{div}\,\mathbf{V}) + \omega^2(\rho_{12}\mathbf{U} + \rho_{22}\mathbf{V}) \\ \qquad = \mathrm{o} \qquad (4b) \end{cases}$$

where the dissipative term b is included in the complex unit masses ρ_{mn}:[12]

$$\rho_{mn} = \tilde{\rho}_{mn} + (-1)^{m+n}\frac{ib}{\omega}. \tag{5}$$

Equation (4) is expressed in terms of fluid and solid displacements, which sum up to six variables. As mentioned by Bonnet,[13] eqn (4) can be condensed in terms of four variables, including three components of solid displacement, U and one scalar S proportional to fluid pressure P

$$S = -fP = Q\,\mathrm{div}\,\mathbf{U} + R\,\mathrm{div}\,\mathbf{V}. \tag{6}$$

After taking the divergence of eqn (4b)

$$\nabla^2 S + \omega^2\rho_{22}\,\mathrm{div\ V} + \omega^2\rho_{12}\,\mathrm{div\ U} = 0 \tag{7}$$

and after eliminating V and div V from eqns (4a) and (7), the following system of four scalar equations is obtained:

$$\begin{cases} N\nabla^2\mathbf{U} + \left(P - N - \dfrac{Q^2}{R}\right)\mathbf{grad}\,(\mathrm{div\ U}) \\ \qquad +\omega^2\rho\mathbf{U} + \alpha\ \mathrm{grad\ (S)} = 0 \\ \nabla^2 S + \dfrac{\omega^2\rho_{22}}{R}\,\mathrm{S} - \omega^2\rho_{22}\alpha\ \mathrm{div\ U} = 0, \end{cases} \tag{8}$$

where

$$\rho = \rho_{11} - \frac{\rho_{12}^2}{\rho_{22}}, \qquad \alpha = \frac{Q}{R} - \frac{\rho_{12}}{\rho_{22}}.$$

Equation (8) is analogous to the equations of coupled thermoelasticity, after replacing pressure S with temperature T and redefining the physical coefficients. Biot[11] was the first to point out the isomorphism of poroelasticity and thermoelasticity. This physical analogy is extremely valuable for importing analytical solutions from thermoelasticity, the governing equations of which are the objects of theorems of existence and uniqueness (e.g., Cupradze *et al.*[14]).

In axisymmetric dynamic problems, the displacement U is expressed by using the scalar potentials Φ and Ψ (e.g., Morse & Feshbach[15]):

$$\mathrm{U} = \frac{1}{K}\,\mathrm{grad}\,\Phi + \frac{1}{K_t}\,\mathrm{curl}\,(\,\mathrm{curl}\,(\mathbf{r}\Psi)), \tag{9}$$

where r is the radius-vector, and K and K_t are the wave numbers of longitudinal and transverse waves. The wave numbers K and K_t make the displacement vector of eqn (9) dimensionless. After using eqn (9), eqn (8) is satisfied when the following equations are satisfied:

$$N\nabla^2\Psi + \omega^2\rho\Psi = 0 \tag{10}$$

and

$$\begin{cases} M\nabla^2\Phi + \omega^2\rho\Phi + \alpha K S = 0 & (11a) \\ \nabla^2 S + \dfrac{\rho_{22}}{R}\omega^2 S - \dfrac{\rho_{22}}{K}\omega^2\alpha\nabla^2\Phi = 0, & (11b) \end{cases}$$

where $M = P - (Q^2/R)$. Equation (10) is a scalar Helmholtz equation with the following wavenumber:

$$K_t = \omega\sqrt{\frac{\rho}{N}}. \tag{12}$$

Applying operator ∇^2 to eqn (1 la), and eliminating $\nabla^2 S$ and S, eqn (1 la) becomes

$$\nabla^4\Phi + \omega^2 A\nabla^2\Phi + \omega^4 B\Phi = 0, \tag{13}$$

where

$$A = \frac{\rho}{M} + \frac{\alpha^2\rho_{22}}{M} + \frac{\rho_{22}}{R}, \quad \text{and} \quad B = \frac{\rho\rho_{22}}{MR}.$$

Equation (13) can be rewritten in the form

$$(\nabla^2 + K_f^2)(\nabla^2 + K_s^2)\Phi = 0, \tag{14}$$

where

$$\begin{cases} K_f^2 + K_s^2 = A\omega^2 \\ K_f^2 K_s^2 = B\omega^4. \end{cases} \tag{15}$$

According to Boggios' theorem (e.g., Nowacki[16]), Φ is the sum of a fast and slow compressional wave

$$\Phi = \Phi_f + \Phi_s, \tag{16}$$

where Φ_f and Φ_s satisfy the scalar Helmholtz equations with complex wave numbers K_f and K_s

$$K_{f,s} = \frac{\omega^2}{2}(A \pm \sqrt{A^2 - 4B}). \tag{17}$$

The imaginary part of $K_{f,s}$ is selected to be positive so that the wave amplitude decays when $r \to \infty$. Equation (17) is equivalent to the dispersion equation obtained by Biot[11]. S is found directly from eqn (1 la) by using $\nabla^2\Phi = -K^2\Phi$

$$S = \frac{1}{\alpha}\left[(MK_f^2 - \omega^2\rho)\frac{\Phi_f}{K_f} + (MK_s^2 - \omega^2\rho)\frac{\Phi_s}{K_s}\right]. \tag{18}$$

The characteristic frequency ω^* is defined as

$$\omega^* = \frac{b}{\tilde{\rho}} \tag{19}$$

where $\tilde{\rho} = \tilde{\rho}_{11} + 2\tilde{\rho}_{12} + \tilde{\rho}_{22}$. Because the hydraulic conductivity k has small values for most geological media (i.e. k varies from 10^{-2} to 10^{-10} m s^{-1}), $\omega^* \gg 1$, and therefore $\omega/\omega^* \ll 1$ for low harmonic frequencies. Under this condition, eqns 17 and 12 can be asymptotically expanded in terms of w/w*. The first-order term provides us with approximated complex wave numbers for fast, slow and transverse waves:"

$$K_f = w\sqrt{\frac{\tilde{\rho}}{P+2Q+R}} \times \left\{1 + \frac{i}{2}\left(\frac{\omega}{\omega^*}\right)\left(\frac{Q+R}{P+2Q+R}\frac{\tilde{\rho}_{12}+\tilde{\rho}_{22}}{\tilde{\rho}}\right)^2\right\} \tag{20a}$$

$$K_s = (1+i)\sqrt{\frac{\omega\omega^*\tilde{\rho}(P+2Q+R)}{2(PR-Q^2)}} \tag{20b}$$

$$K_t = \omega\sqrt{\frac{\tilde{\rho}}{N}}\left\{1 + \frac{i}{2}\left(\frac{\omega}{\omega^*}\right)\left(\frac{\tilde{\rho}_{12}+\tilde{\rho}_{22}}{\tilde{\rho}}\right)^2\right\}. \tag{20c}$$

Scatter of plane harmonic waves on a spherical poroelastic inclusion embedded in poroelastic space

As shown in Fig. 1, in the space described with spherical coordinates (r, θ, φ), a plane harmonic wave originating far away from the space origin (i.e., $r \to \infty$, $\theta = 180°$) approaches a spherical inclusion of radius a which is located at the origin (i.e. $r = 0$). The incident wave is assumed to be of the fast-compressional type. Slow-compressional waves are excluded because they have a negligible amplitude when they strike the inclusion, owing to their distant origin and strong attenuation. Hereafter, the variables of the inclusion are indexed

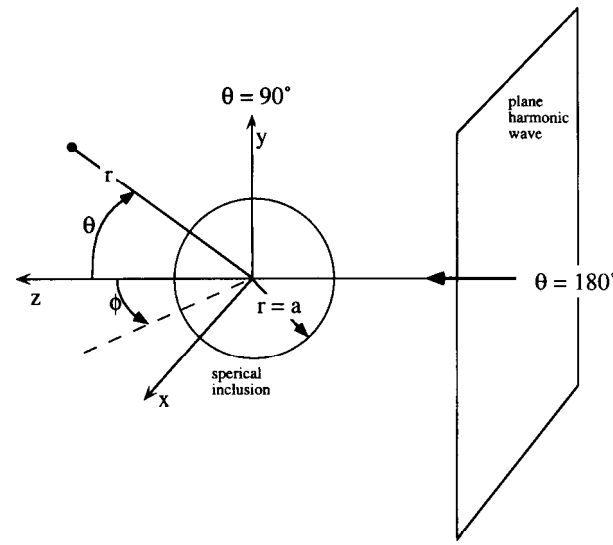

Fig. 1. Schematized representation of the scatter of a plane harmonic wave impinging on a spherical inclusion embedded in an infinite medium.

with i, those of the external medium with e, and those of the incident wave with 0. The displacement vector of the fast incident wave that propagates in the z-axis is

$$\mathbf{u}^0 = \mathbf{e}_z \exp[i(K_{fe}z - wt)], \tag{21}$$

where $\mathbf{e}_z$ is the unit vector along the z-axis, and K_{fe} is the wave number of the incident wave. Since $\mathbf{U}^\circ = \text{grad}\,(\Phi_o)/K_{fe}$, the potential of the incident wave is

$$\Phi_0 = -\sum_{n=0}^{\infty}\Omega_n j_n(K_{fe}r)P_n(\cos\theta) \tag{22}$$

where $\Omega_n = (i)^{n+1}(2n+1)$, $j_n(\,)$ is a spherical Bessel function, and $P_n(\,)$ is Legendre polynomial. Plane waves are represented in terms of spherical functions as described in Morse & Feshbach.[15] The potentials Φ_f, Φ_s and Ψ of eqn (9), which satisfy the Helmholtz equation, are written in terms of spherical coordinates

$$\Phi_{fe,fi} = \sum_{n=0}^{\infty}\Omega_n A^n_{fe,fi} b_n(K_f r)P_n(\cos\theta)$$

$$\Phi_{se,si} = \sum_{n=0}^{\infty}\Omega_n A^n_{se,si} b_n(K_s r)P_n(\cos\theta) \tag{23}$$

$$\Phi_{te,ti} = \sum_{n=0}^{\infty}\Omega_n A^n_{te,ti} b_n(K_t r)P_n(\cos\theta),$$

where constants A^n are determined from boundary conditions; $b_n(Kr) = h_n^{(1)}(K_e r)$ describes the wave in the surrounding media in terms of a spherical Hankel function of the first kind; and $b_n(Kr) = j_n(K_i r)$ describes the waves in the inclusion in terms of $j_n(\cdot)$. Angle φ is omitted in eqn (23) due to axisymmetry.

The boundary conditions on the spherical interface at

$r = a$ are (e.g Bourbié *et al.*[17]):

$$U_r^0 + U_r^e = U_r^i \tag{24a}$$

$$U_\theta^0 + U_\theta^e = U_\theta^i \tag{24b}$$

$$\sigma_{rr}^0 + S^0 + \sigma_{rr}^e + S^e = \sigma_{rr}^i + S^i \tag{24c}$$

$$\sigma_{r\theta}^0 + \sigma_{r\theta}^e = \sigma_{r\theta}^i \tag{24d}$$

$$f_e[(U_r^0 + U_r^e) - (V_r^0 + V_r^e)] = f_i(U_r^i - V_r^i) \tag{24e}$$

$$i\omega f_i(V_r^i - U_r^i) = \chi\left[\frac{S^i}{f_i} - \frac{S^e + S^0}{f_e}\right]. \tag{24f}$$

Equation (24a, b) expresses the continuity of radial and tangential displacements on the interface at $r = a$. Equation (24c, d) represents the continuity of the total stress $\bar{\boldsymbol{\sigma}}$ at $r = a$, where $\bar{\boldsymbol{\sigma}}$ is the sum of the effective normal stress $\boldsymbol{\sigma}$ transmitted by the elastic skeleton and the pore fluid pressure S

$$\bar{\boldsymbol{\sigma}} = \boldsymbol{\sigma} + S\mathbf{I}, \tag{25}$$

where I is the unit tensor. Equation (24e) expresses the continuity of filtration velocity $f(\dot{\mathbf{V}} - \dot{\mathbf{U}})$ in the direction normal to the interface. Similar to Darcy's law, eqn (24f) controls the fluid flow through the interface, and states the proportionality of pressure difference and filtration velocity. The material constant χ characterizes the interface permeability. When $\chi \to \infty$, the interface is pervious, and the fluid pressure is identical on each side of the interface (i.e., $\Delta S = 0$). When $\chi = 0$, the interface is impervious, and the interstitial fluid does not flow across the interface.

By using eqn (4b), the fluid pseudo-displacement V is calculated in terms of the fluid pressure and solid displacement

$$\mathbf{V} = -\frac{\rho_{12}}{P22}\mathbf{U} - \frac{1}{\omega^2 P22}\,\mathbf{grad}\, S. \tag{26}$$

The total stress is defined by using the constitutive equations of poroelasticity, which becomes after elimination of V

$$\bar{\sigma}_{rr} = \left(P - 2N - \frac{Q^2}{R}\right)\operatorname{div}\mathbf{U} + 2N\frac{\partial U_r}{\partial r} + \left(1 + \frac{Q}{R}\right)S$$

$$\bar{\sigma}_{r\theta} = N\left(\frac{1}{r}\frac{\partial U_r}{\partial \theta} + \frac{\partial U_\theta}{\partial r} - \frac{U_\theta}{r}\right). \tag{27}$$

By using eqns (9), (18), (23), (26) and (27) and after straight-forward calculations, the poroelastic solutions become

$$U_r = \sum_{n=0}^{\infty}\Omega_n[A_f^n D_1(K_f r) + A_s^n D_1(K_s r) + A_t^n D_2(K_t r)]\, P_n(\cos\theta)$$

$$U_\theta = \sum_{n=1}^{\infty}\Omega_n[A_f^n D_3(K_f r) + A_s^n D_3(K_s r) + A_t^n D_4(K_t r)] \times \frac{dP_n(\cos\theta)}{d\theta}$$

$$V_r = -\sum_{n=0}^{\infty}\Omega_n[g_f D_1(K_f r)A_f^n + g_s D_1(K_s r)A_s^n + g_t D_2(K_t r)A_t^n]P_n(\cos\theta)$$

$$S = \frac{Mr}{\alpha}\sum_{n=0}^{\infty}\Omega_n\left[\left(K_f^2 - \frac{\rho\omega^2}{M}\right)D_3(K_f r)A_f^n + \left(K_s^2 - \frac{\rho\omega^2}{M}\right)D_3(K_s r)A_s^n\right]P_n(\cos\theta) \tag{28}$$

$$\bar{\sigma}_{rr} = \frac{2N}{r}\sum_{n=0}^{\infty}\Omega_n[D_5(K_f r)A_f^n + D_5(K_s r)A_s^n + D_6(K_t r)A_t^n]P_n(\cos\theta)$$

$$\bar{\sigma}_{r\theta} = \frac{2N}{r}\sum_{n=1}^{\infty}\Omega_n[D_7(K_f r)A_f^n + D_7(K_s r)A_s^n + D_8(K_t r)A_t^n]\frac{dP_n(\cos\theta)}{d\theta},$$

where

$$D_1(z) = nD_3(z) - b_{n+1}(z),$$

$$D_2(z) = n(n+1)D_3(z),$$

$$D_3(z) = \frac{b_n(z)}{z},$$

$$D_4(z) = D_1(z) + D_3(z),$$

$$D_5(z) = \left(n^2 - n + h_{f,s}\frac{z^2}{2}\right)D_3(z) + 2b_{n+1}(z), \tag{29}$$

$$D_6(z) = n(n+1)D_7(z)$$

$$D_7(z) = (n-1)D_3(z) - b_{n+1}(z),$$

$$D_8(z) = \left(n^2 - 1 - \frac{z^2}{2}\right)D_3(z) + b_{n+1}(z),$$

$$g_{f,s} \frac{\rho}{P22}\frac{\rho_{12}}{\alpha\rho_{22}} - \frac{MK_{f,s}^2}{\alpha\omega^2 P22}, \qquad g_t = \frac{\rho_{12}}{\rho_{22}}$$

$$h_{f,s} = \frac{M}{\alpha N}\left(1 + \frac{\rho_{12}}{\rho_{22}}\right) - \frac{Q+R}{R\alpha}\frac{K_t^2}{K_{f,s}^2}.$$

After substituting the general solutions of eqn (28) into the boundary conditions of eqn (24), and using the orthogonality properties of Legendre polynomials, a

system of six linear equations with six unknowns A^n_{fe}, A^n_{fi}, $A^n_{se}, A^n_{si}, A^n_{te}$ and A^n_{ti}, is obtained for each value of n.

The main quantities of interest in soil dynamics are the solid displacements in the far field (i.e. at a significant distance from the spherical inclusion). In this case $Re(Kr) \gg 1$, and Hankel functions can be approximated as follows:

$$h^{(1)}_n(z) \approx \frac{1}{z}(-i)^{n+1}e^{iz}.$$

After neglecting the terms of r^{-2} order, the displacement vector becomes

$$\begin{aligned} U^e_r &\approx iF_f(\theta)\frac{a}{r}e^{iK_{fe}(r-a)} + iF_s(\theta)\frac{a}{r}e^{iK_{se}(r-a)} \\ U^e_\theta &\approx iF_t(\theta)\frac{a}{r}e^{iK_{te}(r-a)}, \end{aligned} \tag{30}$$

where F_f, F_s and F_t are the scattering amplitudes associated with the fast, slow and transverse waves, respectively:

$$\begin{aligned} F_f(\theta) &= \frac{e^{iK_{fe}a}}{K_{fe}a}\sum_{n=0}^{\infty}(2n+1)P_n(\cos\theta)A^n_{fe} \\ F_s(\theta) &= \frac{e^{iK_{se}a}}{K_{se}a}\sum_{n=0}^{\infty}(2n+1)P_n(\cos\theta)A^n_{se} \\ F_t(\theta) &= \frac{e^{iK_{te}a}}{K_{te}a}\sum_{n=0}^{\infty}\left(2n+1\right)\frac{dP_n(\cos\theta)}{d\theta}A^n_{te} \end{aligned} \tag{31}$$

Dynamic viscoelasticity and viscoelastic approximation of poroelasticity

In linear Kelvin-Voigt materials without body forces, the field equations are

$$\left[(\lambda+2\mu)+(\lambda_v+2\mu_v)\frac{\partial}{\partial t}\right]\mathbf{grad}\,(\mathrm{div}\,\mathbf{u}) - \left(\mu+\mu_v\frac{\partial}{\partial t}\right)\mathbf{curl}\,(\mathbf{curl}\,(\mathbf{u})) = \tilde{\rho}\ddot{\mathbf{u}}, \tag{32}$$

where λ and μ are Lame elastic moduli, λ_v and μ_v are the viscous moduli, and $\tilde{\rho}$ is the unit mass of viscoelastic material. In the case of harmonic analysis [i.e., eqn (3)], eqn (32) becomes

$$(\lambda+2\mu)(1-i\omega\xi_{dv})\,\mathbf{grad}\,(\mathrm{div}\,\mathbf{U}) - \mu(1-i\omega\xi_{tv})\,\mathbf{curl}\,(\mathbf{curl}(\mathbf{U})) + \tilde{\rho}\omega^2\mathbf{U} = \mathbf{0} \tag{33}$$

where $\zeta_{tv} = \mu_v/\mu$ and $\zeta_{dv} = (\lambda_v + 2\mu_v)/(\lambda+2\mu)$. By using eqn (9), it can be shown that the scalar potentials Φ and Ψ in viscoelasticity also satisfy Helmholz equations

$$(\nabla^2 + K^2_{dv})\Phi = 0, \quad \text{and} \quad (\nabla^2 + K^2_{tv})\Psi = 0, \tag{34a}$$

where the complex wave numbers are

$$K^2_{dv} = \frac{\omega^2}{C^2_{dv}(1-i\omega\xi_{dv})}, \quad K^2_{tv} = \frac{\omega^2}{C^2_{tv}(1-i\omega\xi_{tv})},$$

and

$$C^2_{dv} = \frac{\lambda+2\mu}{\tilde{\rho}}, \quad C^2_{tv} = \frac{\mu}{\tilde{\rho}}. \tag{34b}$$

The direct comparison of eqns (10), (14) and (34a) establishes that dynamic poroeiasticity and viscoelasticity obey the same Helmholtz equation with different shear and dilatational wave numbers, provided that we neglect the slow poroelastic wave with wave number K_s. Hereafter, the poroelastic-viscoelastic similarity is defined by equating the poroelastic and viscoelastic wave numbers for shear and dilatational waves. The wavenumbers of dilatational (K_{dv}) and shear (K_{tv}) waves of the equivalent-viscoelastic medium are

$$K_{dv} = K_f, \quad \text{and } K_{tv} = K_t \tag{34c}$$

where K_f and K_t are the corresponding poroelastic wave numbers. In general, the moduli of the equivalent-viscoelastic material are frequency-dependent. However, for small attenuation and frequencies, the equivalent-viscous material becomes frequency independent. When $\omega\xi_{dv} \ll 1$ and $\omega\xi_{tv} \ll 1$, eqn (34b) becomes

$$\begin{aligned} K_{dv} &\approx \frac{\omega}{C_{dv}}\left(1+\frac{i}{2}\omega\xi_{dv}\right) \\ K_{tv} &\approx \frac{\omega}{C_{tv}}\left(1+\frac{i}{2}\omega\xi_{tv}\right). \end{aligned} \tag{35}$$

When the following condition is met:

$$\frac{\omega\tilde{\rho}}{b} \ll 1 \tag{36}$$

the equivalent-viscoelastic material becomes the linear Kelvin-Voigt material, and the viscosities and attenuations of the shear and dilatational waves in this equivalent medium can be calculated from poroelastic properties: [10]

$$\begin{cases} C_{dv} = \sqrt{\dfrac{P+2Q+R}{\tilde{\rho}}} \\ C_{tv} = \sqrt{\dfrac{N}{\tilde{\rho}}} \\ \xi_{dv} = \dfrac{\tilde{\rho}}{b}\left(\dfrac{Q+R}{P+2Q+R} - \dfrac{\tilde{\rho}_{12}+\tilde{\rho}_{22}}{\tilde{\rho}}\right)^2 \\ \xi_{tv} = \dfrac{\tilde{\rho}}{b}\left(\dfrac{\tilde{\rho}_{12}+\tilde{\rho}_{22}}{\tilde{\rho}}\right)^2. \end{cases} \tag{37}$$

The viscoelastic-poroelastic similarity is valuable to develop new numerical and analytical methods for solving poroelastic problems. Some approximate methods can easily be derived from elasticity solutions. For

instance, the problem of wave scatter on a spherical inclusion has a well-known solution when the inclusion and matrix are both purely elastic.[2] This elastic solution was extended to viscoelasticity by using the correspondence principle,[18] after replacing the real wave numbers by complex ones (e.g., Gaunaurd & Überall[3] and Morochnik[4]). This viscoelastic solution can then be applied to poroelastic media by invoking the viscoelastic-poroelastic similarity. In the scatter of viscoelastic waves by a spherical inhomogeneity, the boundary conditions enforce the continuity of the stress components σ_{rr} and $\sigma_{r\theta}$, and that of the displacement components u_r and u_θ on the interface at $r = a$. There are now only four boundary conditions, instead of the six equations of poroelasticity [i.e. eqn (24)], because there are no longer drainage conditions.

APPLICATIONS TO WAVE SCATTERING PROBLEMS IN SATURATED SOILS

In geophysical applications, the scatter of waves that impinge on an inclusion are generally determined far away from the inclusion. These scattering effects can be evaluated by computing the scattering amplitudes of eqn (31).

Numerical implementation

In theory, the scattering amplitudes in poroelastic materials can easily be calculated after implementing eqn (3 1) in a computer code. However, in practice, these computations are impeded by numerical difficulties which arise from the large imaginary part of slow wave numbers K_s. As shown in eqn (20b), real and imaginary parts of K_s are practically equal and reach very large values, especially when $k \ll 1$, which makes the calculation of spherical Bessel functions $j_n(K_s r)$ and $h_n^{(1)}(K_s r)$ extremely difficult. These difficulties were circumvented by using the ratio of Bessel functions

$$\psi_n^i(z) = z\frac{j_{n+1}(z)}{j_n(z)}$$
$$V\%(z) = z\frac{h_{n+1}^{(1)}(z)}{h_n^{(1)}(z)}, \tag{38}$$

where the recurrence relations for $\psi_n(z)$ are

$$\psi_{n+1}(z) = 2n + 3 - \frac{z^2}{\psi_n(z)} \tag{39}$$

and

$$\psi_0^i(z) = 1 - \text{zcotan(z)}, \quad \text{and} \quad \psi_0^e(z) = 1 - iz.$$

After solving the linear system of equations [i.e. eqn (24)] with Cramer's Rule, the scattering coefficients of eqn (31) become

$$A_{fe}^n = \frac{j_n(z_{fe})\,\Delta_n^f(\omega)}{h_n(z_{fe})\,\Delta_n(\omega)}$$
$$A_{se}^n = \frac{j_n(z_{fe})\,z_{se}\,\Delta_n^s(\omega)}{h_n(z_{se})\,z_{fe}\,\Delta_n(\omega)} \tag{40}$$
$$A_{te}^n = \frac{j_n(z_{fe})\,z_{te}\,\Delta_n^t(\omega)}{h_n(z_{te})\,z_{fe}\,\Delta_n(\omega)},$$

where z = Ka; **A**, and $\Delta_n^{f,s,t}(\omega)$ are the determinants dependent only on the ratio of Bessel functions. The term $h_n(z)$ in the denominators of eqn (40) and the factor e^{iz} in eqn (31) cancel each other, which eliminates catastrophic over- and under flows in the computations. The series in eqn (31) converges very quickly with n. The terms in the series were retained as long as the ratio of the current term to the sum of the previous terms was larger than 10^{-5}. The number N_{max} of terms necessary to reach such an accuracy was empirically evaluated by using the following relation:

$$N_{max} \approx z_{fe} + 4\sqrt[3]{z_{fe}} + 4. \tag{41}$$

Numerical results

The viscoelastic approximation of poroelastic solutions was tested by examining four particular combinations relevant to geophysical applications. These combinations include three extreme types of saturated soils — gravel, sand, and clay. Biot's material parameters are calculated based on the assumption that solid grains are much more incompressible than the interstitial fluid and grain skeleton:[6]

$$\begin{cases} Q = (1-f)D_f \\ R = fD_f \\ P = D + \dfrac{(f-1)^2}{f}D_f \\ N = \dfrac{D}{3}, \end{cases} \tag{42}$$

where D_f is the fluid bulk modulus, and D is the elastic bulk modulus of the grain skeleton. Equation (42) assumes that Poisson ratio ν is equal to 0.25. The fluid mass coefficient $\tilde{\rho}_{12}$ which takes very small values (e.g., Zimmerman & Stern') is neglected. The unit masses $\tilde{\rho}_{11}$ and $\tilde{\rho}_{22}$ are related to ρ_s and ρ_f — the unit mass of solid and fluid constituents, respectively — through:

$$\begin{cases} \tilde{\rho}_{11} = (1-f)\rho_s \\ \tilde{\rho}_{22} = f\rho_f \\ \tilde{\rho}_{12} = 0. \end{cases} \tag{43}$$

The numerical values of constants for soils, which are listed in Table 1, are taken from Bardet.[10] The interstitial fluid is assumed to be pure water with the following properties: $D_f = 2000$ MPa and $\rho_f = 1000$ kg m^{-3}. The

Table 1. Material properties used in analyses

Properties of material	Type of material		
	Gravel	Sand	Clay
Porosity, f	0·2	0·4	0·5
Elastic stiffness, $\boldsymbol{D}$ (MPa)	200	50	0·05
Poisson ratio, ν	0·25	0·25	0·25
Solid constituent unit mass, ρ_s (kg m^{-3})	2600	2600	3000
Hydraulic conductivity, k (m s^{-1})	10^{-3}	10^{-5}	10^{-10}
Velocity of fast compressional wave, c_f (m s^{-1})	2115	1605	1414
Attenuation of fast compressional wave at ω = 1 cps, ξ_f (s)	$6{\cdot}7 \times 10^{-5}$	3.6×10^{-8}	$5{\cdot}0 \times 10^{-12}$
Velocity of slow compressional wave at w = 1 cps, c_s (m s^{-1})	3.13	0.04	$1{\cdot}5 \times 10^{-5}$
Velocity of shear wave, c_t (m s^{-1})	175	90	2·9
Attenuation of shear wave at ω = 1 cps, ξ_t (s)	$4{\cdot}4 \times 10^{-5}$	$4{\cdot}1 \times 10^{-8}$	5.0×10^{-12}

wave velocities and attenuations of Table 1 are calculated for poroelastic properties, and cover typical ranges of velocity and attenuations for soils. The computations were carried out by setting the radius $\boldsymbol{a}$ of the inclusion equal to 100 m, which is an upper bound for the size of inclusion in soils. However, the numerical results, being dimensionless, apply to other values of a. The effect of the drainage conditions were also investigated in poroelastic calculations by considering impervious (i.e. $\chi = 0$) and pervious (i.e. $\chi = \infty$) interfaces.

As previously mentioned, our analysis is limited to an incident fast-compressional plane wave. At the impact on the inclusion, this wave is scattered into a combination of fast, slow, and transverse (shear) waves. The fast, slow and transverse waves that are scattered in the direction θ are characterized by scattering amplitude $F_f(\theta), F_s(\theta)$, and $F_t(\theta)$, respectively, which are referred to as fast-to-fast, fast-to-slow and fast-to-transverse scattering amplitudes. The wave scatter will be examined in the directions θ = 180" and 90°, which corresponds to back- and side-scatters, respectively. The converted-mode scatter, which transforms fast waves into slow waves, is not covered here. Such a converted-mode scatter generates waves much smaller than fast-to-fast and fast-to-transverse scatter. The fast-to-transverse scatter will be examined in the direction θ = 90" perpendicular to the propagation direction of the incident wave; there is no fast-to-transverse scatter for θ = 180" due to $P_n^1(\cos(\pi)) = 0$.

Figures 2-5 show the fast-to-fast scattering amplitude $|F_f|$ for θ = 180" for the following cases: sand inclusion in gravel matrix, gravel inclusion in sand matrix, sand inclusion in clay matrix and clay inclusion in sand matrix. The variation of $|F_f|$ is represented as a function of the dimensionless frequency $Re(K_{fe}a)$ which covers a wide frequency range of interest to soil dynamics. When K_{fe} can be approximated by using eqn (20a), $Re(K_{fe}a)$ becomes equal to $\omega a/c_{fe}$. $|F_f|$ was found to be practically identical for impervious (χ = 0) and pervious (χ = cc) interfaces. The drainage conditions on the inclusion interface do not influence the scattering amplitude of poroelastic media in the far field. Figures 2-5 clearly illustrate the diversity and complexity of back-scatter in poroelastic media which arises from the large impedance contrast between soil-inclusion and soil-matrix. The oscillations of response curves result from the interference of the waves that are diffracted from the interface, and transmitted through the inclusion (i.e. refracted). As shown in Fig. 3, for a gravel inclusion,

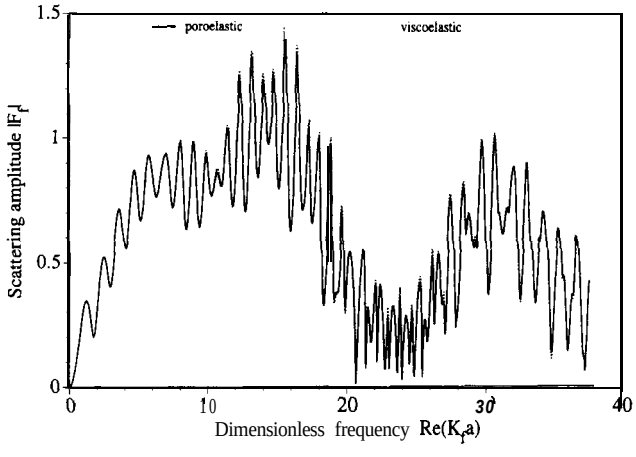

Fig. 2. Poroelastic and equivalent-viscoelastic variation of scattering amplitudes $|F_f|$ vs dimensionless frequency for θ = 180" and a spherical sand inclusion embedded in a gravel matrix.

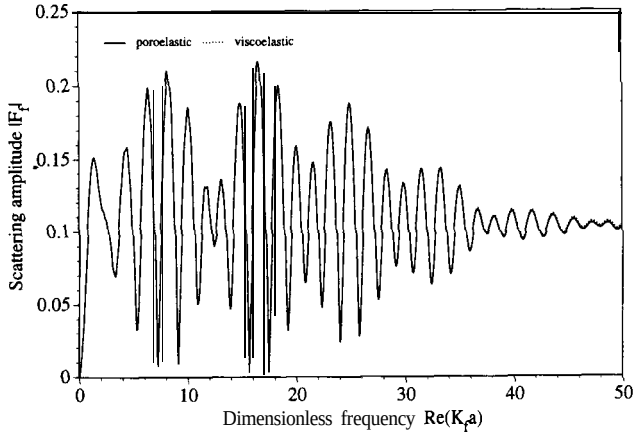

Fig. 3. Poroelastic and equivalent-viscoelastic variation of scattering amplitudes $|F_f|$ vs dimensionless frequency for θ = 180" and a spherical gravel inclusion embedded in a sand matrix.

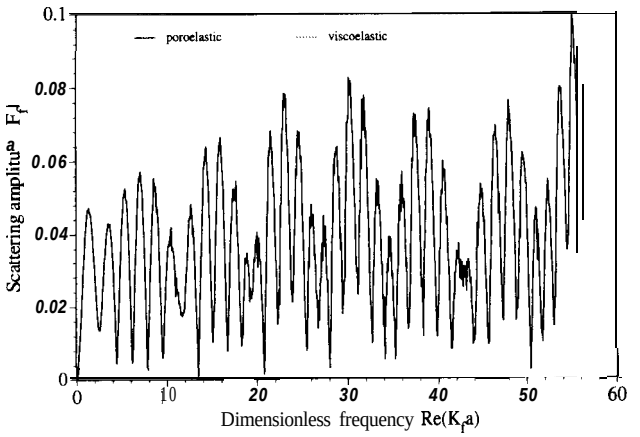

Fig. 4. Poroelastic and equivalent-viscoelastic variation of scattering amplitudes $|F_f|$ vs dimensionless frequency for θ = 180" and a spherical sand inclusion embedded in a clay matrix.

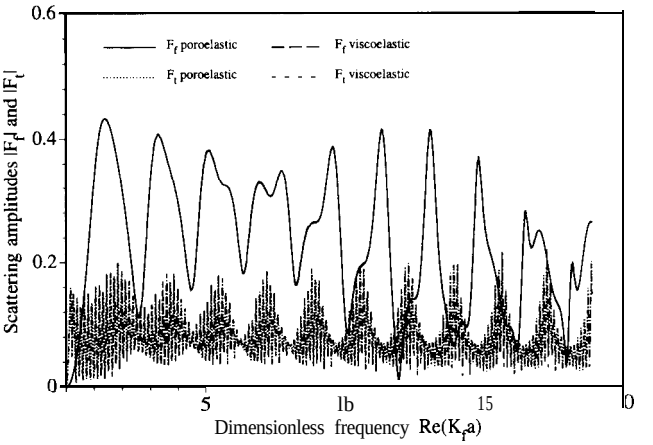

Fig. 6. Poroelastic and equivalent-viscoelastic variation of scattering amplitudes $|F_f|$ and $|F_t|$ vs dimensionless frequency for θ = 90" and a spherical sand inclusion embedded in a gravel matrix.

these oscillations decay with high frequencies because the refracted high-frequency waves are strongly attenuated in the inclusion, and no longer interfere with the diffracted waves. Also shown in Figs 2-5, the back-scattering amplitude is small when the waves are faster in the inclusion than in the matrix, and conversely, becomes large when the waves are slower in the inclusion than in the matrix. In the case of high-frequencies, when the wavelength of incident waves is negligible compared to the inclusion radius a (i.e. $Re(K_{fe}a) \gg 1$), these results can be explained by using optical geometry. According to Snell's law, when the rays are much faster in the inclusion than in the matrix, most of the incident rays are refracted, first into the inclusion, but almost parallel to its interface, and then into the matrix. These refracted rays do not penetrate deep enough into the inclusion for their propagation direction to be reversed by reflection on the interface. In this case, the back-scattering amplitude is small. In contrast, when the ray velocity is smaller in the inclusion than in the matrix, the incident rays go into the inclusion, and can reverse their propagation direction owing to reflections. In this case, reflected and diffracted rays interfere, and the back-scattering amplitude become significant.

Figures 6 and 7 show the transverse scatter for a sand inclusion in the gravel matrix, and ***vice-versa,*** for a gravel inclusion in a sand matrix. In these two cases, the fast-to-fast and fast-to-transverse scattering amplitudes $|F_f|$ and $|F_t|$ are represented as functions of $Re(K_{fe}a)$. Similar to back-scatter, side-scatter in the far field is not influenced by the drainage conditions on the inclusion interface. The fast-to-transverse scattering amplitude $|F_t|$ appears to oscillate more rapidly with frequency than fast-to-fast scattering amplitude $|F_f|$ because the horizontal scale in Figs 6 and 7 is normalized with the fast wave velocity, which is faster than the shear wave velocity (see Table 1). The fast-to-transverse scattering amplitude is generally smaller than the fast-to-fast scattering amplitude, except for low frequencies.

The scattering amplitudes were independently

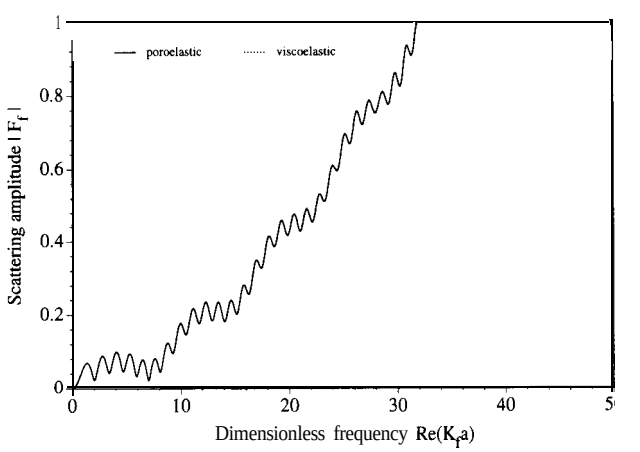

Fig. 5. Poroelastic and equivalent-viscoelastic variation of scattering amplitudes $|F_f|$ vs dimensionless frequency for θ = 180" and a spherical clay inclusion embedded in a sand matrix.

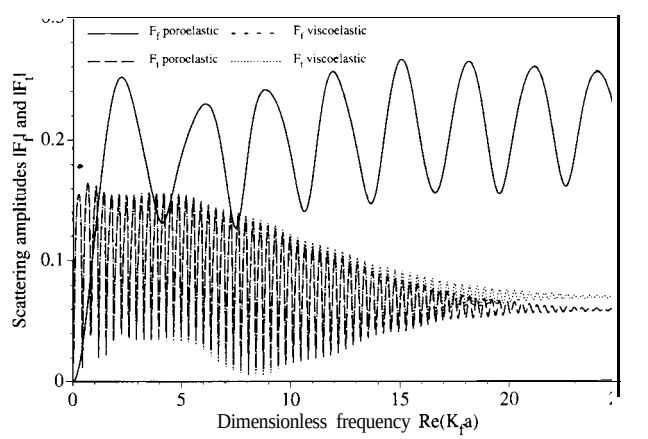

Fig. 7. Poroelastic and equivalent-viscoelastic variation of scattering amplitudes $|F_f|$ and $|F_t|$ vs dimensionless frequency for θ = 90" and a spherical gravel inclusion embedded in a sand matrix.

calculated for equivalent-viscoelastic media as described by Morochnik.[4,19] This numerical technique, which is simpler than that for poroelastic media, is not detailed here. In the low-frequency region (i.e. $w < 0.1b/\tilde{\rho}$), the wave numbers K_{dv} and K_{tv} of the equivalent-viscoelastic material were calculated from the poroelastic properties by using eqns (35) and (37), whereas for higher frequencies, K_{dv} and K_{tv} were calculated by using eqns (12) and (17). The latter equations were only used for gravel in which the limit frequency $\omega_1 = 0.1b/\tilde{\rho} \approx 20$ cps is exceeded.

As shown in Figs 2-7, the scattering amplitudes for poroelastic media are practically identical with those of equivalent-viscoelastic material. Indeed, the agreement is so close that it is impossible to distinguish poroelastic and equivalent-viscoelastic responses. Figure 7 shows only a slight difference in the fast-to-transverse scatter, in the high-frequency range for a gravel inclusion embedded in a sand matrix.

DISCUSSION OF RESULTS

As previously mentioned, the preceding numerical examples show that the scatter of waves in the far field is not influenced by the drainage conditions on the inclusion interface [i.e. eqns (24e,f)]. This result is beneficial to the viscoelastic representation of poroelastic media which cannot account for the drainage boundary conditions. However, the drainage has non-negligible effects in the proximity of the inclusion, and in the farfield when $b = 0$. This latter instance corresponds to the particular case of non-dissipative poroelastic media with a superpermeability (i.e., $b = 0$ and $k \to \infty$), which is an exceptional case in soil dynamics beyond the scope of this paper.

From a physical point of view, the viscous–porous similarity could be useful for examining the specific features of poroelasticity which do not exist in viscoelasticity, namely, to detect the effects of the slow-compressional waves. There are controversies about the physical origins and consequences of the slow wave in poroelastic materials, which are fueled by the lack of experimental data.[20] The slow wave has only been measured at high frequencies (500 kHz) in saturated fused-glass beads, but not yet in other materials such as rocks and soils.[21] In default of direct measurement, the poroelastic–viscoelastic comparison could help to investigate the existence of the slow waves in soils and rocks by detecting some of its specific effects. This work is however beyond the scope of the present study.

This paper shows that the scattering of waves in poroelastic and viscoelastic media share similar features over a wide range of frequency. This similarity is useful to develop approximate analytical viscoelastic solutions for various types of engineering problems, which are difficult to extract from poroelasticity. Such analytical solutions are instrumental to verify the finite elements and finite difference solutions of the propagation of small amplitude waves in saturated soils. The analytical solution of viscoelastic scattering can also be used in the geophysical detection of underground objects buried in saturated soils, and changes in permeability after grouting. The scattering on spherical inclusions needs to be extended to elliptical inclusions, which are a first-order representation of saturated soil lenses embedded in soil of contrasting permeability and stiffness.

The viscoelastic approximations can also be used to investigate poroelastic effects in the spectral analysis of surface waves (SASW) which are deployed for determining the shear wave profile of soil layers.[22,23] The solution of scattering problems on the inclusions of various geometrical shapes may provide us with an understanding of the large viscous damping which was reported for small strain amplitude shaking of saturated soils (e.g., Elgamal *et al.*[24]).

CONCLUSION

The viscoelastic nature of dynamic poroelasticity was called upon to propose a simplified and approximate method for solving dynamic problems in poroelastic media. This method relies on equivalent-viscoelastic materials that have the same wavenumbers as the poroelastic media. In the particular problem of scatter of plane compressional waves by a spherical poroelastic inclusion, the poroelastic and equivalent-viscoelastic solutions were found to be practically identical far away from the inhomogeneity. The proposed method adds to our existing numerical and analytical methods for poroelastic media, and is useful to derive approximate and simplified solutions for wave scattering problems in soil dynamics and geophysics.

ACKNOWLEDGEMENTS

The financial support of the Air Force Office of Scientific Research (grant F49620-93-1-0295) is acknowledged. The authors are thankful to J. Young for her help in typing the manuscript, and to M. Harris for proofreading the manuscript.

REFERENCES

1. Sivukhin, D., Diffraction of a plane wave by spherical cavity (in Russian) *Akusticheskiy Zhurnal*, *1955*, 1, 78–88.
2. Ying, C. F. & Truell, R., Scattering of a plane longitudinal wave by a spherical obstacle in an isotropically elastic solid, J. *Appl. Phys.*, 1956, *17*, 1086–1097.
3. Gaunaurd, G. & Überall, H., Theory of resonant scattering from spherical cavities in elastic and viscoelastic media, *J. Acoust. Soc. Am.*, 1978, 63, 1799–1712.

4. Morochnik, V., Wave scattering by a spherical inclusion in viscoelastic media, *Zzvestya, Phys. Solid Earth, 1987, 23,* 159–161.
5. Berryman, M., Scattering by a spherical inhomogeneity in a fluid-saturated porous medium, *J. Math. Phys., 1985, 26,* 1408–1419.
6. Biot, M. &Willis, D., The elastic coefficient of the theory of consolidation, *J. Appl. Mech. ASME, 1957, 24,* 594–601.
7. Zimmerman, C. & Stern, M., Scattering of plane compressional waves by spherical inclusion in a poroelastic medium, *J. Acoust. Soc. Am.,* 1993, 94, 527–536.
8. Kargl, S. & Lim, R., A transition-matrix formalism for scattering in homogeneous saturated porous media. *J. Acoust. Soc. Am.,* 1992, **94**, 1527–1550.
9. Zimmerman, C. & Stern, M. Analytical solutions for harmonic wave propagation in poroelastic media, *J. Engng. Mech., 1994, 120, 215442178.*
10. Bardet, J. P., A viscoelastic model for the dynamic behavior of saturated poroelastic soils, *J. Appl. Mech. ASME, 1992, 59,* 128–135.
11. Biot, M. A., Theory of propagation of elastic waves in a fluid-saturated porous solid, *J. Acoust. Soc.* Am., 1956, 28, 168-191.
12. Norris, A. N., Radiation from a point source and scattering theory in a homogeneous, saturated porous media. *J. Acoust. Soc.* Am., 1985, 77, 2012–2023.
13. Bonnet, G., Basic singular solution for a poroelastic medium in the dynamic range, *J. Acoust. Soc. Am., 1987, 82,* 1758–1762.
14. Cupradze, V. D., Gegelya, T. G., Basheleishvili, M. 0. & Burchuladze, T. V., *Three-dimensional Problems of Mathematical Theory of Elasticity and Thermoelasticity.* (in Russian). University Press, Tbilisi, Georgia, Russia, 1968.
15. Morse, P. M. & Feshbach, H., *Methods of Theoretical Physics.* McGraw-Hill, New York, 1953.
16. Nowacki, W., *Theory of Elasticity* (in Russian), Mir Ed., Moscow, Russia, 1975, pp. 568.
17. Bourbié, T., Coussy, 0. & Zinszner, B., *Acoustics of Porous Media* Gulf Publishing, Houston, Texas, 1987.
18. Eringen, A. C., *Mechanics of Continua.* Krieger, New York, 1980.
19. Morochnik, V., Scattering of compressional waves by a low-contrast spherical inclusion, *Zzvestya, Phys. Solid Earth, 1983, 19, 548-553.*
20. Bardet, J. P., The damping of saturated poroelastic soils during steady state vibrations, *Appl. Math. Comput., 1994, 67, 3-31.*
21. Plona, T. J., Observation of a second bulk compressional wave in a porous medium at ultrasonic frequencies, *Appl. Phys. Lett., 1980, 36, 259-261.*
22. Nazarian, S. & Stokoe II, K. H. *In-Situ* shear wave velocity from spectral analysis of surface waves, *Proc. 8th World Conf. on Earthquake Engineering,* Vol. 3, 1984, pp. 31–38.
23. Tokimatsu, K., Tamura, S. & Kojima, H., Effects of multiple modes on Rayleigh wave wave dispersion, *ASCE J. Geotech. Engng., 1992,* 118, 152991543.
24. Elgamal, A. W., Seghal, M. & Parra, E., Identification and modeling of earthquake ground response, *Proc. 1st Int. Conf. on Earthquake Geotechnical Engineering,* IS-Tokyo, Tokyo, Japan, pp. 51-90, 1995.